THE ASTROPHYSICAL JOURNAL, 347:251–265, 1989 December 1

THE NONTHERMAL STELLAR DYNAMICS OF THE GLOBULAR CLUSTER M15[1]

RUTH C. PETERSON[2]
Whipple Observatory, Smithsonian Astrophysical Observatory
PATRICK SEITZER[2]
Space Telescope Science Institute
AND
KYLE M. CUDWORTH
Yerkes Observatory, University of Chicago
Received 1987 March 17; accepted 1989 May 30

ABSTRACT

The velocity dispersion as a function of radius in the globular cluster M15 is derived from measurements of 120 individual stars between 0.'1 and 4.'6 of the cluster center, and from the integrated light of the central cusp. The stellar measurements, with an individual accuracy of 1 km s^{-1}, indicate a mean cluster velocity of -107.1 ± 0.9 km s^{-1}, and a mean velocity dispersion of 9.0 ± 0.6 km s^{-1}. The velocity dispersion inside 1′ varies with radius. The dispersion of the 27 stars within 20″ is 14.2 ± 1.9 km s^{-1}, while that of the 30 stars between 0.'5 and 1.'2 is 8.4 ± 1.4 km s^{-1}. The cusp itself appears to have a dispersion of at least 25 km s^{-1}. Except for its greater velocity broadening, the spectrum of the integrated light of the cusp is indistinguishable from that formed by superposition of the individual M15 giant spectra, demonstrating that the excess light at the center is due primarily to a normal M15 population.

The increase of the dispersion toward the center is not consistent with truncated isothermal (King-Michie) models, for which the velocity dispersion is nearly constant within a few core radii and then falls steeply beyond. The observed behavior is difficult to reconcile as well with current post–core collapse models, which are also isothermal and whose central energy sources are modest. It is indicative of a nonthermal energy distribution with substantial heating in the central regions; this is consistent with a central black hole of about 1000 $M_\odot$.

Subject headings: clusters: globular — radial velocities — stars: stellar dynamics

I. INTRODUCTION

The globular cluster M15 is the classical cusp cluster. Instead of following a normal King (1966) model profile, its luminosity profile shows excess central light (Newell and O'Neil 1978; Djorgovski and King 1984; Hertz and Grindlay 1985). The innermost region also harbors both a bright X-ray source (Hertz and Grindlay 1983) and a millisecond pulsar (Wolszczan *et al.* 1989); both are believed to arise from the hard binary systems formed in high stellar densities. The cusp itself was originally suggested as the signature of a black hole (Newell, Da Costa, and Norris 1976) or of a central condensation of neutron stars (Illingworth and King 1977). Current theoretical work favors post–core collapse of ordinary stars, with a central energy source fuelled by binaries (Spitzer 1985; Heggie 1985; Cohn 1985).

It has long been realized that knowledge of the stellar dynamics of M15 would constrain these models. Since the central relaxation time is several orders of magnitude less than a Hubble time, and the tidal radius is large, the region interior to about 30″ in M15 is expected to be in thermal equilibrium. This is the prediction of both single and multimass King models, as well as existing post–core collapse models, except for a brief reversal of the core collapse in the latter. Since thermal equilibrium demands that the velocity dispersion of any mass group should be constant in the central regions, only the black hole scenario currently allows the velocity dispersion to rise within 30″ of the center; in this case a sharp increase is predicted (Cohn 1985).

Previous observations of the dynamics of this cluster are sketchy (King 1985). The cluster was not included by Illingworth (1976) in his determination of the central velocity dispersions of southern globular clusters from integrated light. Cudworth (1976) marginally detected the velocity dispersion in his study of proper motions. Accurate radial velocity measurements for individual stars have been published for only five members (Peterson, Olszewski, and Aaronson 1986). The dearth in radial velocity measurements has largely been due to the extreme metal deficiency of the cluster (Buonanno, Corsi, and Fusi Pecci 1985, Table 1).

In this paper we present radial velocities good to 1 km s^{-1} for 120 cluster members and the dispersion of the central cusp from the line breadth of lines in the spectrum of the integrated light. We use these to derive the velocity dispersion as a function of distance from the cluster center and compare these with model predictions. We first discuss our CCD frames of the central region in various bandpasses (§ II), to identify the cusp region and illustrate the difficulties with crowding there. In § III we describe the new high-resolution spectra, and the derivation of individual stellar radial velocities and their uncertainties via cross-correlation techniques. In § IV, spectra of the

[1] Research based on observations obtained with the Multiple Mirror Telescope, a joint facility of the Smithsonian Institution and the University of Arizona.

[2] Visiting Astronomer, Kitt Peak National Observatory, National Optical Astronomical Observatories, operated by the Associated Universities for Research in Astronomy, Inc., under contract with the National Science Foundation.

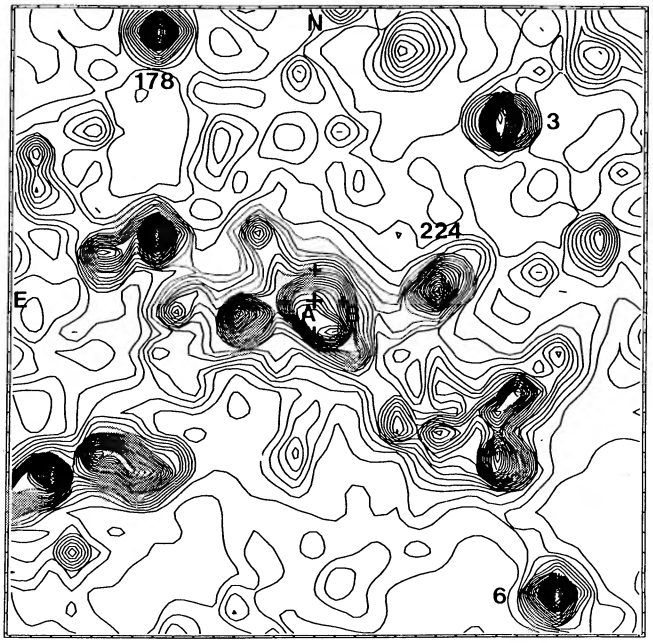

FIG. 1.—An isocontour map in V light is presented of the center of M15. The field shown is 17″ × 17″, and is taken from a 2 s exposure on the KPNO 4 m with a Fairchild CCD. Positions of the central spectra are marked; the large cross is position C, and the small crosses are the points observed 0.″8 away in each direction. The circle around the northern cross indicates a 1.″2 aperture. Numbers adjacent to several stars are AC identifications.

cluster center itself are introduced, and the central velocity dispersion is found from the breadth of the cross-correlation peak. Various characteristics of the deduced velocity dispersion are discussed in § V. In § VI, the resulting run of velocity dispersion as a function of radius is described and compared to theoretical model predictions.

II. CCD IMAGES AND THE POSITION OF THE CLUSTER CENTER

To identify as precisely as possible the position of the cluster center with reference to the individual stars which heavily populate the region, several frames of the innermost region were obtained at the prime focus of the 4 m telescope of Kitt Peak National Observatory by Seitzer. The V and B frames shown in Figures 1 and 2 were obtained in 1987 May with a Fairchild CCD, with a resolution of 0.″54 per pixel. The region shown covers 17″ × 17″. The K frame shown in Figure 3 was obtained in 1988 May with the InSb infrared array camera, and a sampling of 0.″3 per pixel. Individual stars are identified there according to Aurière and Cordoni (1981, hereafter AC) and Aurière, Le Fèvre, and Terzan (1984).

The central region in V light was recorded by McClure, Racine, and Christian (1989) at a FWHM resolution of 0.″36, by stopping the CFHT aperture to an effective 1.2 m and using piezoelectric guiding controls. A full-size glossy print of the best image shown in Figure 5 of that paper was kindly provided to us by Bob McClure in 1988 November.

In large-scale V images, the position of the cusp is not obvious, since the center is dominated by several bright stars. In the K band, where the individual giants stand out, a blend of three stars is evident. Although these are partially resolved in the McClure *et al.* V image, the cusp itself is still elusive. It can be discerned by superposing the K and B frames; in the latter,

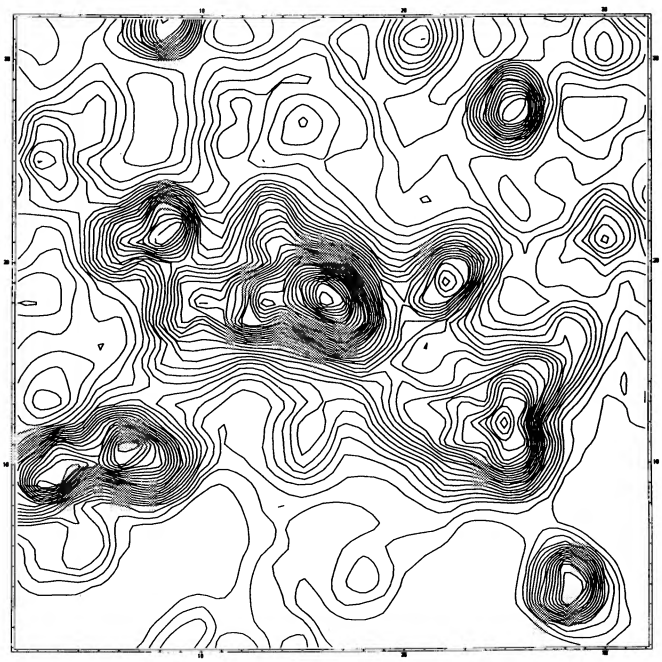

FIG. 2

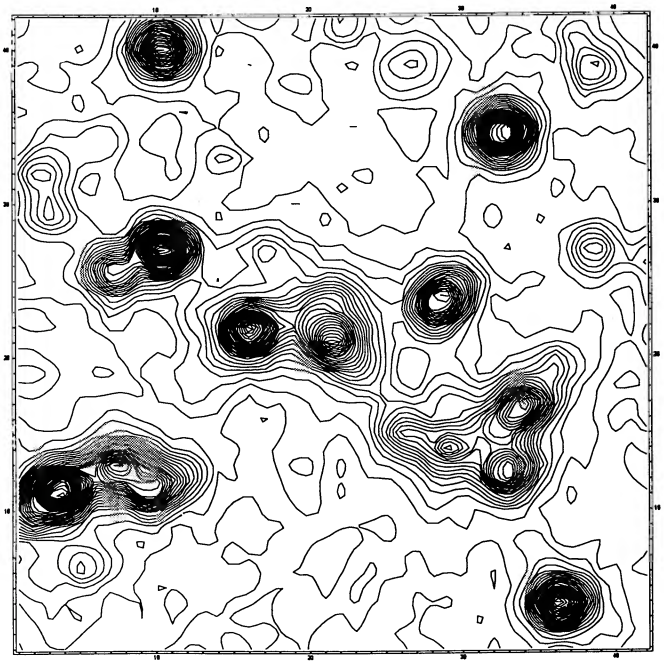

FIG. 3

FIG. 2.—Same field as in Fig. 1 is shown in B light, from a 4 s Fairchild CCD exposure.

FIG. 3.—Same field as in Fig. 1 is shown in K light. This is the median of 10 1 s exposures made at the KPNO 4 m with an InSb Santa Barbara Research Corporation array of 58 × 62 pixels. The brightest stars stand out strongly in this bandpass.

a new peak or plateau appears about 0".8 to the northeast of the K brightness peak. This coincides with a 1" by 0".5 gap between the central stars in the McClure *et al.* frame, where the background light also is quite strong. The gap is centered 0".4 WNW of the large cross in Figure 1.

Our frames suggest that the background light has an integrated V magnitude of roughly 13, and a color of $B-V = 0.9 \pm 0.1$, based on photometric calibration of these frames by standard stars. To within the large uncertainties due to crowding, our measurements are consistent with the magnitudes for stars in the region listed by Aurière *et al.*

Both the magnitude and the color of the cusp region are consistent with a clump of giants 2–3 mag fainter than the tip of the M15 giant branch. The spectrum reported below supports this also.

III. STELLAR SPECTROSCOPY

a) Mount Hopkins Echelles

A total of 119 stars in the field of M15 and the central light of the cluster were observed with the echelle spectrographs of the Multiple Mirror Telescope (MMT) and 1.5 m Tillinghast reflector of the Whipple Observatory, on Mount Hopkins, Arizona. Spectra for 79 members, two nonmembers, and the cluster center were obtained by Seitzer and Peterson on the MMT during 1986 July 24–29 (UT). An additional 10 members near the center were observed by Peterson on the 1.5 m telescope 1986 November 11–12, and four more by Lee Hartmann on the MMT 1986 November 11. During 1987 May 10–11 Cudworth and Peterson obtained 14 observations of central stars. On 1988 July 27 Peterson repeated 13 of these and obtained velocities for 10 additional ones within 10" of the center. During each run, the M15 star K144 (Küstner 1921) = II-75 (Arp 1955) was observed repeatedly as a velocity standard.

As described by Latham (1985), the configuration of the echelle spectrograph and intensified Reticon detector is very similar on the two Mount Hopkins telescopes. The major difference is that an image stacker with 1".2 effective apertures is used on the MMT, while a single slit 1" wide is employed at the 1.5 m. Throughout all runs, the 50 Å spectral range was centered between 5180 Å and 5200 Å. An exposure level of about 10 counts per pixel ($=1.35$ km s^{-1}) was typically obtained. A Th-A source was recorded for 90 s at intervals of typically 25 minutes, never exceeding 35 minutes. The mean width in pixels of the comparison-source lines was constant to 5% throughout each run and from run to run, averaging 6.5 pixels at the MMT and 4.9 pixels at the 1.5 m; thus the FWHM resolution of the spectrograph was 9 km s^{-1} at the MMT and 6.5 km s^{-1} at the 1.5 m.

Stellar positions were obtained from PDS measurements by Cudworth to a small fraction of an arcsecond. This, coupled with the ability of the MMT to point to 0".1 throughout the M15 field, enabled short setup times, typically 12 s between the end of one stellar exposure and the beginning of the next. This accuracy also made it possible to unambiguously set up on the desired star, even in the central region, where crowding is so severe that an error of <1" can cause the wrong star to be observed (see Fig. 3). On the 1.5 m during 1986 November 11–12, the TV guider screen was photographed whenever a crowded star was observed, to avoid ambiguity in stellar identifications.

Exposure times at the MMT in 1986 July were typically 12 minutes for a $V = 14.0$ star under excellent conditions. In 1986 November the MMT exposures averaged 18 minutes at $V = 14.0$, while the 1.5 m exposures were generally 15 minutes at $V = 13.3$. Seeing was the crucial issue in runs where central stars were observed. In 1988 July seeing initially was poor, about 2", and gradually improved to 1". To confirm that central velocities were not affected by this seeing, one of the fainter stars, AC 4 with $V = 13.8$, was observed at the beginning and end of that night. The velocities agreed to 0.1 km s^{-1}.

b) Kitt Peak Spectroscopy

Additional echelle spectra were obtained by Seitzer during 1987 July 2–3 UT on the 4 m telescope of Kitt Peak National Observatory. In contrast to the Mount Hopkins observations, which refer to a single position, the KPNO spectra were made with a long-slit and a CCD detector, which retains spatial information. The red long-focus camera and the TI2 CCD with 2×2 and 3×2 binning resulted in a spectral resolution of 10.8 km s^{-1} (4.34 km s^{-1} per pixel), with the 316 lines mm^{-1} echelle grating blazed at 63° and a 150 μm = 1".0 slit. The Mg b line at 5187 Å was centered in the spectral region, which was 30 Å wide.

This sample includes eight stars in common with the MMT runs and three stars otherwise unobserved. Three stars were observed twice, and six spectra were obtained of the standard K144. Exposure times averaged 10 minutes at $V = 13.0$, and 1" seeing prevailed both nights. Th-Ar comparison spectra were obtained at intervals of 20 minutes or less.

c) Spectral Reductions

The reduction of the Mount Hopkins echelle data followed the standard procedure (Tonry and Davis 1979; Wyatt 1985). This consists of dividing the spectrum of each object (and Th-Ar) by a long exposure of an incandescent lamp obtained at the beginning or end of each night; combining the Th-Ar exposures acquired before and after the object exposure to establish a fifth-order terrestrial dispersion solution (based on 30 lines, with an individual line position measured to about 0.02 Å); and applying this to the object. In these reductions, the inherent continuum falloff induced by vignetting and the echelle blaze function was not rectified, to insure that the local level of signal-to-noise ratio (S/N) is appropriately taken into account. After discarding edge pixels seriously affected by distortion, about 1900 pixels remained.

The KPNO spectra were reduced with standard IRAF procedures on the KPNO Sun workstations. After flat-fielding with a quartz exposure, a Th-Ar dispersion solution was applied. The reduced spectra were padded to 512 pixels and written to FITS-format tapes. These were converted on the Nova computer to Mount Hopkins format for subsequent cosmic-ray removal and correlation.

d) Cross-Correlation against Metal-poor Templates and Calculation of Random Error

All velocities were determined by cross-correlation on the Mount Hopkins Nova computer systems (Tonry and Davis 1979). This approach computes the cross-correlation function of the Fourier transforms of a stellar spectrum and a template, a high S/N spectrum of a star of similar spectral type whose radial velocity is known. The displacement of the peak of the correlation function gives the velocity of the star relative to the template, and the uncertainty in this velocity is determined quantitatively from the ratio R of the correlation-peak height

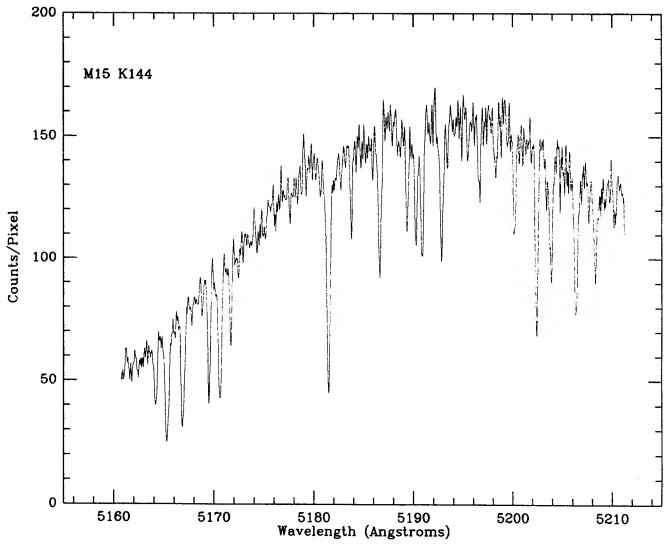

FIG. 4.—The spectrum is shown of the co-addition of 13 MMT observations of the M15 giant K144 = II-75. In this and the following figures, the wavelength scale is terrestrial; the geocentric velocity of about -120 km s^{-1} shifts lines blueward from their rest positions by about 2 Å. The continuum shape is due to the blaze function of the echelle spectrograph.

to that of random noise fluctuations as $\sigma_R = K/(1 + R)$ km s^{-1}.

This formula with $K = 8.3$ applies for sharp-lined spectra obtained with the Mount Hopkins echelles (Peterson 1983; Pryor, Latham, and Hazen 1988). Tonry and Davis (1979) argue that K is proportional to the number of independent resolution elements contained in the spectral range. According to this guideline, K should be a factor of 2 larger for the KPNO data, since spectral coverage is 30 Å rather than 50 Å and spectral resolution is 10.8 km s^{-1} rather than 9 km s^{-1}. The internal agreement of the K144 velocities and the external comparison of velocities of eight stars in common with the MMT data sets confirm that $K = 16$ for the KPNO data. For either setup, intrinsic broadening by an internal dispersion will increase K by the ratio of true line breadth to sharp-line breadth. Using these factors, the velocity error in an individual measurement was calculated; except where otherwise noted, the result was divided by $N^{1/2}$ in cases where N observations of the same object were obtained, to obtain the velocity error of the mean. These are given in § III*e* below and in the tables.

Since the M15 giants are so metal-poor, we used only weak-lined templates for these correlations. Four of the six observations of star K144 itself were used for the KPNO observations. For the Mount Hopkins data, where the S/N of an individual spectrum is considerably lower, four metal-poor templates were generated by combining spectra obtained during the 1986 July MMT run. One was formed from 13 individual spectra for M15 K144; this spectrum is reproduced in Figure 4. Another was produced from 13 spectra obtained for the M22 giant III-93, the velocity standard for the M22 data obtained concurrently by Peterson and Cudworth (1989). The remaining two templates were constructed by combining the spectra for different giants. One of these composite spectra, shown in Figure 5, includes 59 members of M15 more distant than 70″ from the cluster center. The other incorporates 20 stars between 30″ and 90″. For use with M22 but not here, a fifth, higher S/N template was generated by combining 74 M22 stars observed during the same run. None of the five co-added spectra is degraded in resolution by the change in geocentric velocity over the course of the run, which was 0.64 km s^{-1}. However, the three multistar spectra are significantly broadened by the internal stellar velocity dispersion. This was determined explicitly from the individual velocities to be ± 6.2 km s^{-1} for the outer M15 stars, ± 9.3 km s^{-1} for the inner ones, and ± 5.6 km s^{-1} for the M22 stars. Last, for a better visual comparison with the central spectrum, the spectrum of Figure 5 was broadened by an additional dispersion of 15 km s^{-1}, as shown in Figure 6.

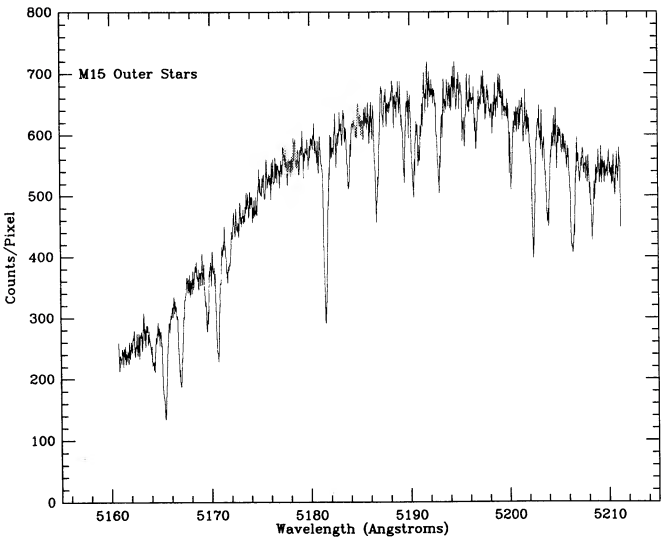

FIG. 5

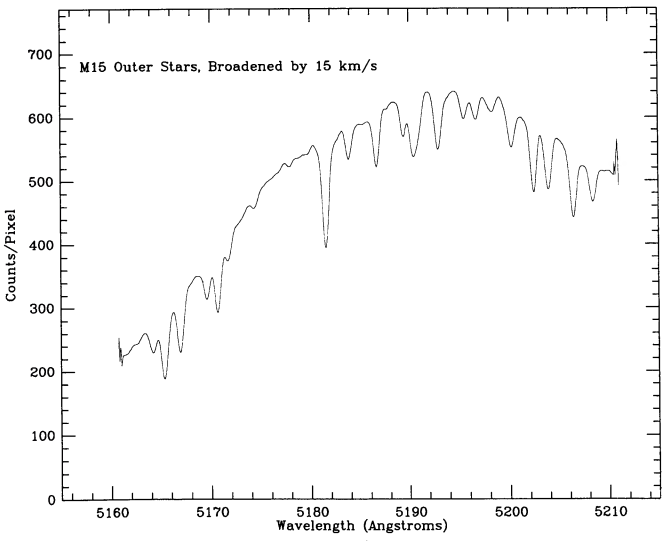

FIG. 6

FIG. 5.—The spectrum is shown of the co-addition of the spectra of 59 stars farther than 70″ from the center of M15. Line profiles are shallower and broader here than in Fig. 4, due to the intrinsic stellar dispersion of 6.2 km s^{-1}.

FIG. 6.—The spectrum of Fig. 5 is shown after broadening by an additional dispersion of 15 km s^{-1}, for comparison with the central spectrum of Fig. 8.

e) Velocity Zero Point

The fundamental zero point for the Mount Hopkins data was set by recording the spectrum of the dawn and dusk sky at both the zenith and at 25° elevation whenever possible. For the 19 sky exposures obtained during the 1986 July MMT run, the uncertainty in the sky zero point is calculated from $\sigma_R/N^{1/2}$ to be ± 0.14 km s^{-1}. For the 1986 November 1.5 m run, six sky exposures yielded ± 0.09 km s^{-1}. During 1987 May, the 17 MMT sky exposures gave a calculated uncertainty of ± 0.14 km s^{-1}. In all cases, the empirical scatter of sky velocities within a run is consistent with the $\sigma_R/N^{1/2}$ values quoted. Although the use of the sky risks a normalization error due to the uniform illumination of the slit, contemporaneous measurements of various velocity standards throughout many MMT and 1.5 m runs shows that this error is small, ≤ 0.5 km s^{-1}, according to Latham (1985).

During all three runs, repeated observations were made for one M15 giant, K144 = II-75. Thirteen measurements of K144 made at the MMT during 1986 July yielded -111.03 ± 0.20 km s^{-1}; three 1.5 m velocities gave -109.17 ± 0.56 km s^{-1}; six MMT velocities from 1987 May averaged -111.14 ± 0.40 km s^{-1}. There is no significant evidence for velocity variability of this star, though changes of 1 km s^{-1} cannot be ruled out. The 22 measurements from the three runs, spanning 300 days, average -110.80 ± 0.19 km s^{-1} with an empirical error per observation of $\sigma_e = 0.97$ km s^{-1}. This is in excellent agreement with the calculated uncertainties, which average $\sigma_R = 0.90 \pm 0.04$.

For the remaining runs, where fewer sky spectra were obtained, K144 was used to set the zero point. After this normalization, the five most accurate KPNO velocities for K144 averaged -110.66 ± 0.54 km s^{-1}, with $\sigma_e = 0.95$ km s^{-1}, and four MMT measures from 1988 July gave -110.75 ± 0.39 km s^{-1}, with $\sigma_e = 0.51$ km s^{-1}. The sky results from four KPNO observations during 1987 July were -1.57 ± 0.74 km s^{-1} with $\sigma_e = 2.02$; those from the MMT in 1988 July were -0.25 ± 0.36 km s^{-1} from three spectra with $\sigma_e = 0.38$. A zero-point uncertainty of ± 0.5 km s^{-1} is thus reasonable to assume for each run. Being of the same order as the above zero-point uncertainties, and much smaller than the random errors, it was ignored in computing the tabulated uncertainties. During Hartmann's run, however, no sky were obtained, and the normalization was made to a single observation of K144, with $\sigma_R = 0.8$ km s^{-1}. We estimate a total uncertainty in this zero point of ± 1.1 km s^{-1}, which was combined in quadrature with the regular σ_R values to produce the final uncertainties listed for K566, K578, K863, and K736 in Table 1 below.

To compare our zero point with that of the CfA system, based also on the sky but on correlations against Population I templates, the 1986 July sky and M15 K144 spectra were correlated in Cambridge using standard procedures there. The zero points agree to 0.05 km s^{-1}, with an uncertainty of 0.2 km s^{-1}.

f) Velocity Results

Table 1 presents our best determinations of velocities for all M15 members observed. The first column gives the mean Julian date of each observation, except for stars observed more than once (see below), where the date of the first observation is listed. The next two columns list right ascension and declination as measured by Cudworth, except that AC coordinates were used for their stars 271, 417, 456, 457, 488, 576, 623, 780, and 787. The next two columns give the radius (in arcminutes) and position angle (in degrees) from the point marked by the large cross in Figure 1. A position of $21^h27^m33^s.33$, $+11°56'48''.8$ (1950) was determined for this, with an absolute uncertainty of $\pm 0''.3$ in each direction. This differs by about 1″ from the position quoted by Hertz and Grindlay (1985) of $21^h27^m33^s.40$, $+11°56'48''.9 \pm 0''.5$. In the sixth column is given the radial velocity. For all multiply-observed stars, this is the weighted mean of the N independent observations in Table 2, except for K912, where the velocity and uncertainty were derived from the single spectrum formed by coadding the two separate exposures; for reasons noted above, the K144 value is the average of 22 of the first 23 exposures (exposure 14 is Hartmann's). The uncertainty, derived as discussed above, appears in the next column. In the eighth column is found the V magnitude, from preliminary measurements by Cudworth except for stars inside 0′.35, where AC values are used. The Küstner (1921) number of each star is found in the next-to-last column, and the roman-numeral designations of Arp (1955), the AC numbers, or the S numbers of Sandage (1970), are given in the last column. Table 2 provides information on the multiple observations which were made for several stars.

Most stars observed were known to be members from the M15 proper-motion study by Cudworth (1976); two which were not included there proved to be nonmembers on the basis of their low radial velocities. Their positions and velocities are listed in Table 3. Brown (1951) also found both to be field stars from his lower precision proper motions. Furthermore, his photometry places both blueward of the cluster giant branch.

IV. LINE STRENGTHS AND BROADENING OF THE CENTRAL SPECTRUM

a) Observations

In 1987 July, four spectra centered on the cusp were obtained at the KPNO 4 m, two spectra in each of two orientations of the slit. On 1987 July 2 the slit position angle was PA = 50°.1, and two 3600 s exposures were obtained displaced 0″.5 apart in 2″ seeing. Binning of 3 × 2 produced 0″.50 per pixel perpendicular to the dispersion. On 1987 July 3, in 1″.5 seeing, binning was 2 × 2, or 0″.34 per pixel along the slit. Exposures of 3000 s and 3600 s were made at PA = 140°.1, again displaced by 0″.5. For all four exposures, a slit 150 μm = 1″.0 wide and 20″.3 long was used, as for the stellar spectra. Figure 7 (Plate 5) shows the PA = 140°.1 spectrum. The central conglomerate of stars covers columns (80)–(90). Star AC 3 falls in columns (107)–(109); its lines are clearly sharp and redshifted with respect to those of the surrounding light, in keeping with its measured velocity, 10 km s^{-1} higher than the cluster mean. Similarly, the lines of AC 111, barely resolved in columns (72)–(74), are blueshifted, and its velocity in Table 1 is 10 km s^{-1} lower than the cluster mean.

At the MMT in 1986 July, four independent observations were obtained of the spectrum of the central light of M15. On July 24 UT the telescope was pointed to position "A" in Figure 1, and two consecutive 25 minute spectra were obtained. The position is known to about 0″.3 in declination and 0″.5 in right ascension with respect to the central cross as deduced from the MMT pointing log. The second night, position "B" west of center was observed twice in succession for 20 minutes apiece.

During 1987 May 10 and 11, position "C" (*large cross*) and

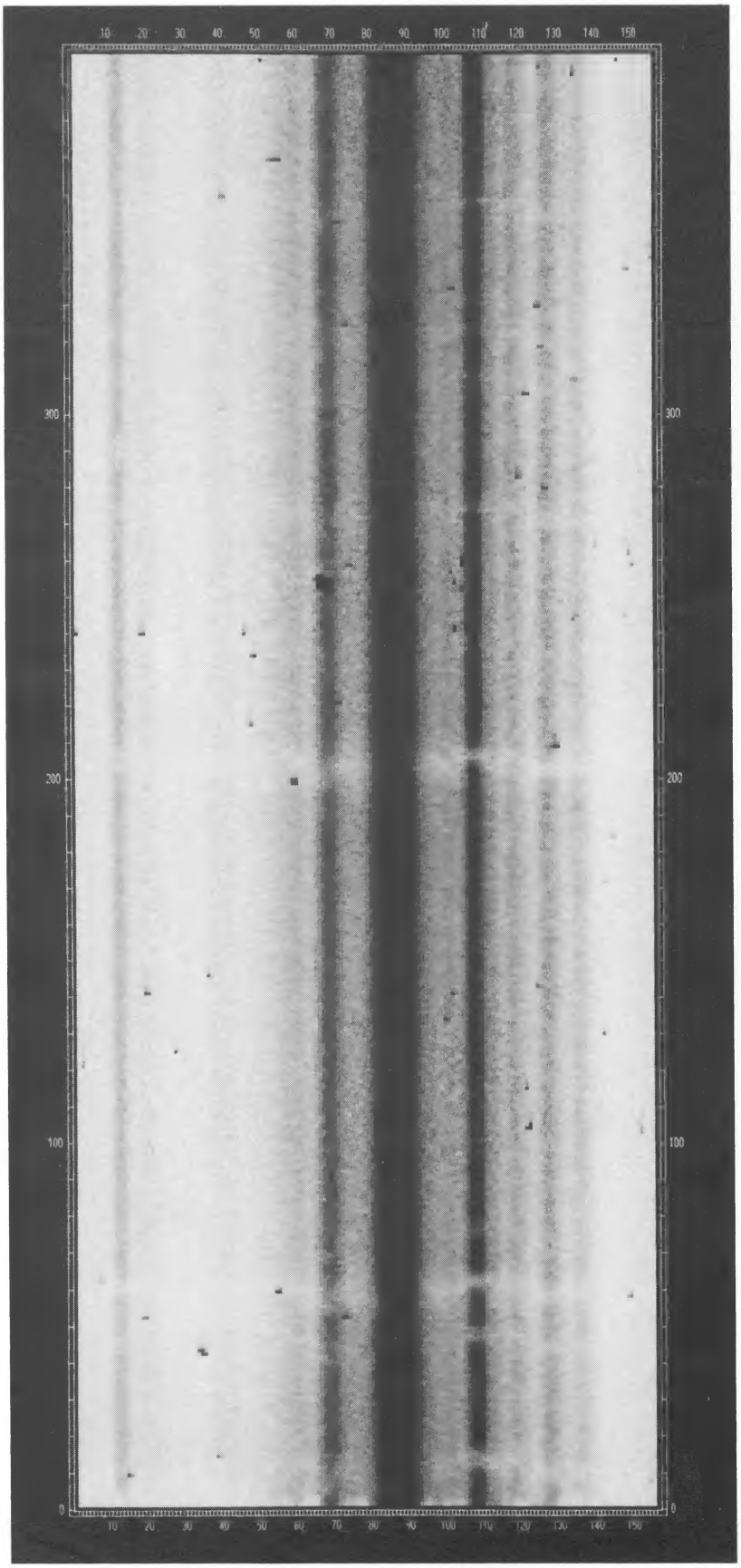

FIG. 7.—A long-slit spectrum of the central region of M15 is shown. This 1 hr exposure was made at the KPNO 4 m with a TI CCD. The slit was oriented at a position angle of 140°1 and passes through the bright star AC 3 of Fig. 1, whose sharp-lined spectrum is easily discerned in columns (107)–(109).

TABLE 1

VELOCITIES FOR M15 MEMBERS

JUL.DATE -2440000	RA (1950)	DEC	R (MIN)	THETA (DEG)	VELOCITY +/- (KM/S)		V	NAME KUSTNER	NAME OTHER
7369.84	21 27 33.42	11 56 48.2	0.03	106.8	-123.93	1.2	13.87		AC212
6979.10	21 27 33.07	11 56 49.0	0.06	274.0	-75.41	1.9	14.09		AC224
6979.09	21 27 33.58	11 56 50.5	0.07	67.9	-97.24	0.9	13.47		AC160
7369.87	21 27 33.66	11 56 50.0	0.09	77.9	-123.25	1.2	13.89		AC161
6927.95	21 27 32.96	11 56 53.5	0.11	313.6	-96.87	1.3	13.47		AC3
6979.11	21 27 32.95	11 56 44.5	0.11	230.0	-107.16	2.2	...		AC253
7369.85	21 27 33.77	11 56 44.1	0.14	124.0	-117.16	0.9	13.33		AC111
6980.25	21 27 33.58	11 56 55.9	0.14	30.2	-92.34	1.0	13.58		AC178
6926.99	21 27 32.85	11 56 40.9	0.17	219.7	-108.88	0.8	13.58	539	AC6
6979.06	21 27 33.97	11 56 44.6	0.18	113.4	-97.61	0.8	13.73		AC104
6927.96	21 27 32.56	11 56 43.0	0.20	242.3	-95.59	0.7	13.66		AC247
6979.07	21 27 34.08	11 56 40.9	0.23	124.7	-86.72	1.3	13.53		AC615
6926.99	21 27 33.10	11 56 34.7	0.24	191.9	-96.68	0.7	13.24		AC414
7369.88	21 27 32.37	11 56 42.1	0.25	243.9	-110.76	1.2	13.94		AC488
7369.90	21 27 32.98	11 57 2.9	0.25	342.0	-83.80	1.3	13.91		AC271
6926.99	21 27 33.31	11 56 33.9	0.25	179.3	-84.96	0.6	13.05	570	AC411
6927.98	21 27 33.36	11 57 3.6	0.25	4.3	-114.20	0.9	13.79		AC780
6927.98	21 27 34.32	11 56 50.9	0.25	82.2	-100.10	0.7	13.50		AC623
7369.89	21 27 33.03	11 57 4.8	0.27	347.0	-115.30	1.7	13.97		AC787
6926.98	21 27 32.88	11 57 4.5	0.28	338.7	-115.88	0.9	13.40		AC1
6927.97	21 27 33.82	11 57 5.2	0.30	25.1	-109.31	0.6	13.45		AC761
6927.97	21 27 32.08	11 56 52.2	0.30	281.0	-125.00	0.7	13.88		AC4
6979.27	21 27 34.55	11 56 46.2	0.31	98.2	-124.21	2.5	14.08		AC576
6927.99	21 27 32.57	11 56 31.9	0.33	212.4	-109.32	1.0	13.22		AC456
6926.98	21 27 33.97	11 57 6.8	0.34	29.1	-123.43	0.7	13.59		AC2
6927.96	21 27 33.20	11 56 28.5	0.34	184.2	-114.15	0.6	13.65	561	AC417
6927.99	21 27 32.48	11 56 32.0	0.34	215.8	-123.08	0.9	13.47		AC457
6640.97	21 27 31.64	11 56 34.4	0.47	239.7	-116.56	0.8	12.95	462	AC13
6640.92	21 27 31.99	11 56 25.6	0.50	219.8	-91.76	0.7	12.86	490	AC463
6746.59	21 27 31.25	11 56 42.5	0.51	258.3	-95.25	1.4	13.48	435	AC529
6745.56	21 27 33.24	11 56 16.2	0.54	181.7	-110.21	1.7	13.85	566	AC407
6640.95	21 27 33.76	11 56 16.4	0.55	168.2	-104.57	0.9	13.11	601	AC12
6640.99	21 27 35.54	11 56 52.1	0.55	84.5	-116.26	1.2	12.96	733	AC11
6745.59	21 27 35.58	11 56 49.4	0.56	89.3	-114.19	1.1	13.18	734	AC650
6640.95	21 27 32.75	11 56 15.9	0.56	193.8	-96.47	0.9	13.04	531	
6640.97	21 27 31.76	11 57 15.0	0.58	319.5	-124.48	1.1	12.65	479	
6635.95	21 27 35.24	11 56 28.9	0.58	125.1	-116.46	0.8	13.06	706	
6640.98	21 27 31.14	11 57 5.9	0.60	298.7	-113.10	0.9	12.73	421	
6640.98	21 27 31.41	11 57 17.5	0.66	316.2	-110.17	1.1	13.16	447	
6640.96	21 27 32.36	11 57 25.9	0.66	340.0	-101.69	1.1	13.11	511	
6640.91	21 27 33.52	11 56 9.3	0.66	175.4	-110.02	1.1	12.89	583	
6745.58	21 27 33.35	11 57 29.6	0.68	1.4	-102.93	1.6	13.72	578	
6745.60	21 27 34.80	11 56 13.7	0.69	148.1	-98.34	1.2	13.13	673	
6745.62	21 27 35.58	11 56 16.3	0.78	134.3	-102.05	1.4	13.92	736	
6640.95	21 27 32.13	11 56 5.5	0.78	201.9	-118.05	1.1	13.11	497	
6745.71	21 27 33.28	11 56 0.7	0.80	180.5	-96.69	1.7	13.17	567	
6640.97	21 27 34.28	11 55 59.5	0.85	164.0	-104.01	0.7	12.77	634	
6635.95	21 27 35.31	11 57 38.7	0.97	30.8	-117.11	0.6	12.98	702	
6636.83	21 27 35.72	11 56 2.7	0.97	142.6	-93.51	1.0	13.46	749	
6745.72	21 27 33.31	11 55 49.9	0.98	179.9	-99.91	2.3	13.66	572	
6635.95	21 27 30.60	11 57 33.6	1.00	318.7	-117.49	0.7	12.83	386	
6640.96	21 27 34.76	11 57 47.9	1.05	20.2	-107.36	0.9	13.02	670	
6745.62	21 27 33.66	11 55 43.9	1.08	175.4	-111.30	1.1	13.37	589	
6745.61	21 27 37.85	11 56 56.2	1.12	83.9	-110.08	1.6	13.83	863	
6745.68	21 27 28.76	11 57 8.5	1.16	286.7	-105.98	1.5	13.64	288	
6745.64	21 27 32.00	11 55 41.1	1.17	195.8	-107.44	1.6	13.39	488	II-16
6745.68	21 27 28.79	11 56 21.9	1.19	248.1	-115.75	1.3	13.28	290	
6639.97	21 27 34.79	11 57 58.7	1.22	17.7	-107.76	1.0	13.74	672	I-6
6635.94	21 27 35.86	11 55 45.0	1.23	149.7	-114.66	0.9	12.83	757	IV-38

TABLE 1—*Continued*

JUL.DATE -2440000	RA (1950)	DEC	R (MIN)	THETA (DEG)	VELOCITY +/- (KM/S)		V	NAME KUSTNER	NAME OTHER
6638.93	21 27 30.45	11 57 52.4	1.27	326.8	-93.93	0.8	12.73	373	
6638.94	21 27 37.71	11 57 31.7	1.29	56.7	-107.78	0.8	12.87	853	
6640.93	21 27 31.89	11 55 32.6	1.31	195.3	-110.83	1.5	14.36	482	III-59
6745.65	21 27 28.27	11 56 22.2	1.31	250.4	-100.73	1.8	13.97	260	
6638.98	21 27 29.68	11 55 47.3	1.35	221.0	-103.17	1.2	13.61	328	III-48
6639.98	21 27 33.31	11 55 27.2	1.36	180.1	-95.96	0.9	13.84	569	III-83
6638.94	21 27 29.41	11 57 50.7	1.40	317.6	-104.84	1.0	13.38	319	
6638.96	21 27 28.54	11 55 58.7	1.43	234.6	-106.93	0.9	13.41	272	III-27
6638.97	21 27 34.41	11 55 23.3	1.45	169.4	-116.02	1.0	13.51	647	
6640.90	21 27 33.69	11 55 20.1	1.48	176.5	-97.45	1.4	13.99	592	IV-65
6636.93	21 27 27.62	11 57 32.2	1.57	297.7	-102.70	0.8	13.17	238	II-29
6638.88	21 27 39.58	11 57 20.5	1.62	71.2	-105.93	1.1	13.76	928	I-43
6635.93	21 27 28.12	11 57 50.8	1.63	309.4	-107.95	0.9	13.25	254	II-31
6640.87	21 27 37.22	11 58 9.5	1.65	35.8	-100.13	0.8	12.80	825	S4,I-12
6637.90	21 27 40.11	11 56 52.0	1.67	88.4	-112.33	0.9	14.24	943	I-38
6635.93	21 27 30.70	11 58 22.0	1.67	338.0	-96.87	0.6	13.20	393	II-42
6637.86	21 27 35.51	11 58 25.0	1.69	18.9	-112.73	1.2	14.22	731	I-63
6639.87	21 27 27.74	11 57 50.1	1.70	307.1	-105.05	0.9	12.89	240	
6636.92	21 27 27.29	11 57 39.7	1.70	300.2	-106.71	0.8	13.32	224	II-30
6638.87	21 27 39.28	11 57 44.0	1.73	58.1	-111.36	1.0	13.50	919	I-50
6638.83	21 27 30.13	11 58 22.4	1.74	333.8	-98.63	1.4	14.42	354	II-40
6637.91	21 27 40.66	11 57 3.5	1.82	82.5	-111.39	1.0	14.09	961	I-41
6640.89	21 27 33.23	11 54 57.2	1.86	180.7	-98.45	1.0	14.51	560	III-70
6637.94	21 27 30.18	11 58 31.4	1.87	336.1	-123.20	1.6	14.50	357	II-44
6639.95	21 27 33.55	11 54 55.8	1.88	178.4	-100.41	1.4	14.48	582	IV-62
6637.86	21 27 40.49	11 55 43.0	2.07	122.1	-101.95	1.2	14.24	954	
6637.84	21 27 39.15	11 55 15.3	2.12	137.6	-101.63	1.1	14.38	912	IV-48
6639.93	21 27 25.24	11 55 51.0	2.19	244.2	-112.96	1.2	14.16	158	III-33
6638.86	21 27 42.28	11 56 25.5	2.23	100.2	-111.04	1.0	13.73	990	IV-10
6637.84	21 27 42.36	11 57 20.8	2.28	76.7	-116.00	1.3	13.92	993	I-74
6635.93	21 27 24.77	11 57 54.2	2.35	297.8	-110.80	0.4	13.05	144	II-75
6635.94	21 27 25.81	11 58 18.5	2.36	309.4	-112.76	0.9	13.35	169	II-64
6637.87	21 27 39.78	11 58 35.0	2.37	42.1	-102.15	1.1	14.44	934	I-62
6637.96	21 27 35.33	11 54 24.1	2.46	168.6	-101.23	0.9	13.53	709	IV-58
6640.88	21 27 26.42	11 54 58.6	2.49	222.8	-106.94	1.2	14.54	185	
6635.92	21 27 31.17	11 59 22.0	2.60	348.7	-107.09	0.7	13.02	431	S1
6636.94	21 27 30.59	11 59 30.6	2.77	346.4	-112.59	0.8	13.36	387	S3
6638.89	21 27 28.10	11 59 19.5	2.81	333.4	-100.34	1.3	13.66	255	
6637.97	21 27 24.89	11 54 53.4	2.81	227.2	-100.65	0.9	13.49	146	S7
6637.98	21 27 22.82	11 55 33.6	2.85	244.2	-112.80	1.0	13.82	114	
6638.85	21 27 42.45	11 55 1.2	2.86	128.9	-112.79	1.0	13.79	994	
6637.88	21 27 44.86	11 57 40.2	2.95	73.4	-111.39	1.1	14.40	1033	
6637.94	21 27 23.61	11 58 34.2	2.95	306.8	-104.64	1.1	14.22	129	
6636.95	21 27 45.45	11 56 53.8	2.97	88.6	-101.24	1.0	13.32	1040	S6
6637.85	21 27 41.90	11 54 34.1	3.07	137.0	-113.72	1.6	14.13	979	
6638.87	21 27 37.72	11 53 43.4	3.27	160.9	-105.94	1.0	13.91	846	
6638.85	21 27 20.78	11 55 33.8	3.31	248.1	-108.95	0.9	13.72	87	S29?
6637.92	21 27 21.07	11 58 20.1	3.35	297.2	-109.66	1.2	14.44	89	
6637.89	21 27 46.33	11 55 28.7	3.45	112.9	-107.05	0.9	14.11	1054	
6639.83	21 27 29.92	12 0 10.8	3.46	346.4	-111.46	0.8	12.79	341	
6636.96	21 27 41.31	11 53 46.8	3.61	147.3	-110.45	0.9	13.35	969	S8
6637.93	21 27 18.50	11 56 51.9	3.62	271.0	-106.97	1.1	14.37	66	S36
6639.89	21 27 38.17	12 0 16.9	3.66	19.2	-110.22	1.1	13.98	875	
6639.90	21 27 40.17	12 0 8.4	3.72	27.0	-119.41	1.1	14.25	947	
6639.88	21 27 43.01	11 59 42.3	3.74	39.7	-113.51	1.4	14.13	1006	
6640.86	21 27 18.74	11 55 21.7	3.84	248.1	-104.01	1.1	14.40	69	
6639.85	21 27 44.77	11 59 42.3	4.03	44.4	-98.55	1.0	14.06	1030	
6639.92	21 27 49.91	11 57 8.3	4.07	85.6	-119.71	1.3	14.12	1073	
6637.97	21 27 19.60	11 54 19.0	4.17	233.6	-103.46	1.0	13.73	77	
6637.90	21 27 50.60	11 55 10.4	4.54	111.4	-106.24	1.0	14.03	1079	
6636.95	21 27 44.70	12 0 30.3	4.62	37.3	-102.81	0.9	13.44	1029	

TABLE 2

STARS WITH MULTIPLE VELOCITY MEASUREMENTS

JUL.DATE -2440000	VELOCITY (KM/S)	+/-	NAME KUSTNER	NAME OTHER
6979.10	-73.93	3.4		AC224
6980.26	-76.08	2.3		
6979.09	-97.79	1.9		AC160
6980.24	-95.08	1.7		
7369.87	-98.09	1.2		
6980.25	-90.49	2.1		AC178
7369.81	-92.94	1.2		
6926.99	-108.85	1.2	539	AC6
7369.75	-108.90	1.0		
6979.06	-98.13	2.4		AC104
7369.85	-97.55	0.8		
6927.96	-96.49	1.1		AC247
7369.81	-94.65	0.8		
6979.07	-90.43	2.9		AC615
7369.86	-85.86	1.4		
6926.99	-96.96	0.9		AC414
7369.77	-96.40	1.0		
6926.99	-85.70	0.7	570	AC411
7369.76	-84.22	1.1		
6927.98	-113.91	1.1		AC780
7369.83	-114.49	1.5		
6927.98	-101.89	1.0		AC623
7369.86	-98.30	1.0		
6926.98	-114.03	1.2		AC1
7369.78	-117.73	1.3		
6927.97	-108.45	1.0		AC761
7369.80	-110.16	0.8		
6927.97	-124.68	1.1		AC4
7369.75	-125.21	1.3		
7369.82	-125.12	1.4		
6927.99	-109.49	1.4		AC456
7369.77	-109.15	1.4		
6927.99	-123.85	1.2		AC457
7369.78	-122.31	1.3		
6926.98	-122.86	0.9		AC2
7369.79	-123.99	1.0		
6927.96	-114.95	0.9	561	AC417
7369.82	-113.34	0.8		
6640.97	-115.74	1.0	462	AC13
6980.08	-117.38	1.3		
6640.92	-91.30	0.8	490	AC463
6980.09	-93.61	1.6		
6640.95	-103.68	1.0	601	AC12
6980.12	-105.45	1.5		
6640.95	-95.26	1.3	531	
6980.10	-97.67	1.1		
6640.97	-102.63	1.0	634	
6745.61	-105.39	1.0		
6640.90	-99.70	1.8	592	IV-65
6640.91	-95.20	2.2		
6635.93	-97.89	0.9	393	II-42
6638.84	-95.85	0.9		
6637.84	-104.62	2.0	912	IV-48
6637.84	-101.21	1.3		
6635.94	-111.34	0.9	144	II-75
6636.94	-111.68	0.7		
6637.84	-111.70	0.8		
6637.88	-111.23	0.8		
6637.95	-110.66	0.8		
6638.82	-109.97	0.9		
6638.90	-110.80	0.7		
6639.84	-111.12	0.7		
6639.90	-111.31	0.8		
6639.96	-110.47	0.8		
6640.86	-112.03	0.8		
6640.95	-110.22	1.1		
6640.98	-110.80	1.0		
6745.55	-110.64	0.8		
6745.57	-110.61	0.7		
6745.75	-109.14	1.3		
6746.57	-107.75	0.8		
6925.96	-111.43	1.0		
6925.99	-111.17	0.8		
6926.94	-111.76	1.0		
6926.97	-110.74	0.9		
6927.00	-110.16	1.5		
6927.95	-111.57	0.8		
6979.05	-107.92	1.9		
6979.13	-109.10	1.2		
6979.24	-111.60	1.2		
6979.25	-111.04	1.2		
6980.06	-111.05	1.2		
6980.27	-110.49	1.2		
7369.74	-110.96	1.0		
7369.78	-110.72	1.0		
7369.83	-111.27	0.7		
7369.88	-110.06	0.6		

four points 0.″8 away in each direction (*small crosses*) were observed. The sequence followed was to observe K144, then C for 6 minutes, then one point 0.″8 away for 5 minutes, then the point 0.″8 away on the opposite side for 5 minutes, then to repeat each observation in reverse order. On May 10, the E and W points were observed, and the N and S on May 11. Seeing was measured at 1″–1.″2 on both nights. The accuracy of these positions relative to the central cross should be 0.″2 in each coordinate, because extreme care was taken to reference the telescope coordinates to the standard K144. Note that the blending of this star with its faint neighbors, noted by Federici *et al.* (1983), is not a problem, since the closest is 3.″8 away (Buonanno *et al.* 1983).

In Figure 8, the A spectrum is shown. Comparison with

TABLE 3

VELOCITIES FOR M15 NONMEMBERS

Julian Date −2,440,000	R.A. (1950)	Decl. (1950)	Velocity (km s^{-1})	V	Küstner Name
6640.92.....	$21^h27^m30^s.40$	11°57′56.″6	−32.88 ± 1.0	14.06	371
6638.90.....	21 27 46.05	11 59 19.8	−37.69 ± 1.2	13.78	1047

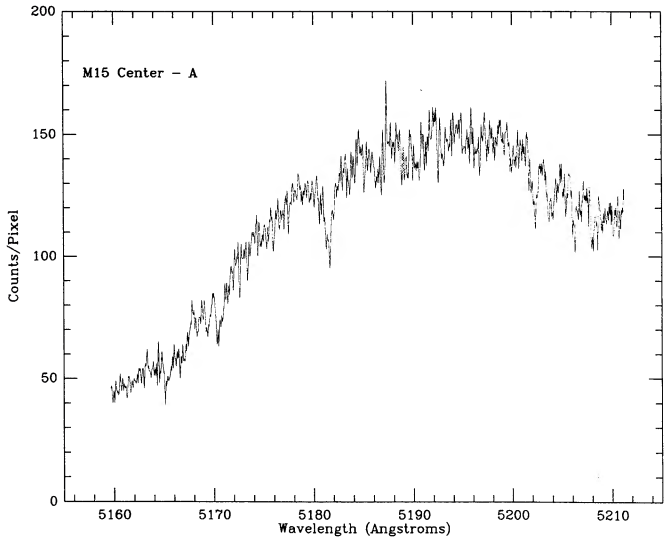

FIG. 8

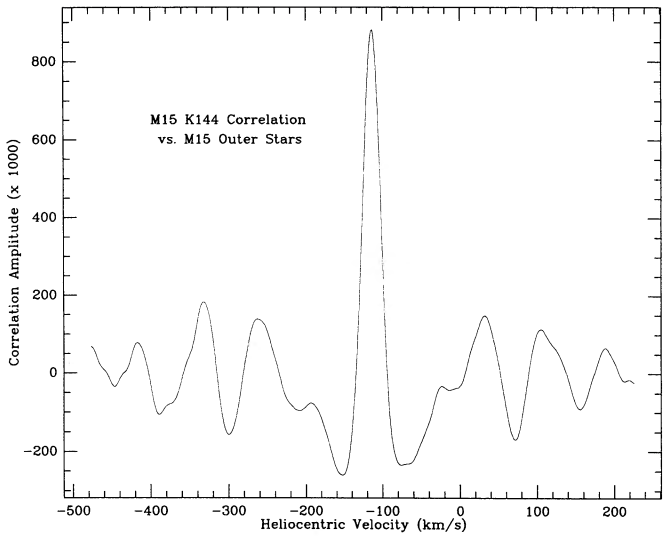

FIG. 9

FIG. 8.—The spectrum formed from the co-addition of two 25 minute exposures is plotted of the integrated light of the center of M15 at position A in Fig. 1.
FIG. 9.—The cross-correlation function is presented of a sharp-lined star observed at high S/N, the template spectrum of M15 K144 (Fig. 4), correlated against the template formed from 59 outer M15 giants (Fig. 5). The peak breadth is measured at 50% of the peak height above the zero level.

Figures 4 and 5 indicates that the central spectrum has unmistakably broader lines than those of a sharp-lined star or the group of outer stars with an intrinsic dispersion of 6 km s^{-1}. Comparison with Figure 6 indicates that the A spectrum is even broader than the spectrum of the outer M15 giants broadened by an additional intrinsic dispersion of 15 km s^{-1}. This is confirmed from the breadth of the correlation peak. Based on the calibration and error analysis discussed below, we present in Table 4 the results for the velocity and velocity dispersion for the coaddition of each MMT spectrum obtained during a single night.

b) Measuring the Breadth of the Cross-Correlation Peak

The use of the breadth of the cross-correlation peak to determine an internal velocity dispersion is illustrated in Figures 9 and 10. Figure 9 shows the cross-correlation function for the sharp-lined star K144 versus the group of outer M15 stars with an intrinsic dispersion of 6 km s^{-1}. Figure 10 shows the cross-correlation of the central A spectrum versus this same template. Clearly its central peak is broader.

Cross-correlation of both high and low S/N spectra of single stars established that, where two sharp-lined stars are correlated, the breadth of the peak is 20.4 km s^{-1} at 50% of its height, and is independent of R value over the range $4 < R < 10$. The breadth is somewhat larger than expected from the 9 km s^{-1} resolution of the MMT echelle convolved with an intrinsic weak-line profile. We attribute this discrepancy to the fact that the peak shape is decidedly non-Gaussian, and depends heavily on the somewhat saturated Mg *b* lines in stars as weak-lined as these.

The quantitative conversion of correlation breadth to a Gaussian dispersion was done by broadening the high signal-to-noise spectra of single stars by Gaussians of known amounts, then correlating these against spectra of single stars to determine the associated breadth. For the MMT spectra, this depended on convolution software written by Neal Burnham of the Center for Astrophysics and modified for a Gaussian velocity distribution. The coadded K144 spectrum of

TABLE 4

MMT CENTRAL SPECTRA

Julian Date −2,440,000	Velocity (km s^{-1})	Dispersion (km s^{-1})	Position
6635.88.....	−116.05 ± 2.2	23.6 ± 3.1	A
6636.85.....	−104.44 ± 1.0	10.1 ± 1.7	B
6925.96.....	−105.57 ± 1.2	8.4 ± 1.5	C
6926.94.....	−108.56 ± 1.6	11.8 ± 1.7	C
6925.97.....	−103.76 ± 1.3	9.3 ± 1.8	0.″8 W
6925.96.....	−116.36 ± 1.2	11.7 ± 1.5	0.″8 E
6926.95.....	−103.32 ± 4.6	30.0 ± 4.3	0.″8 N
6926.95.....	−104.96 ± 1.4	10.1 ± 1.8	0.″8 S

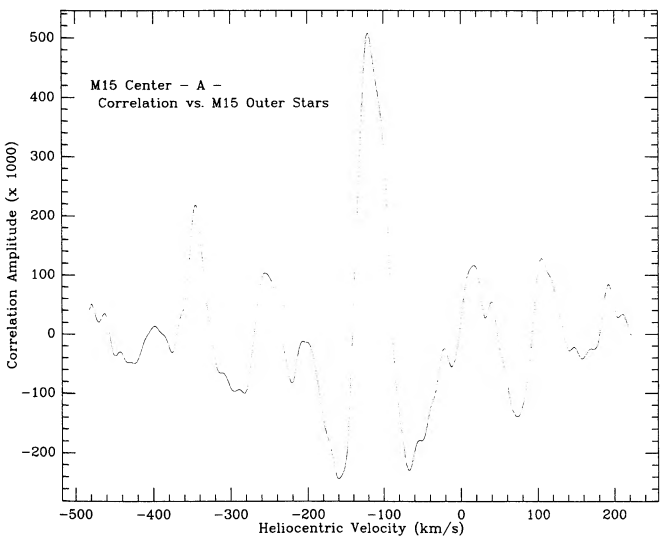

FIG. 10.—The cross-correlation function is presented of the central A spectrum (Fig. 8) against the same template as in Fig. 9. The increased breadth of the peak is apparent.

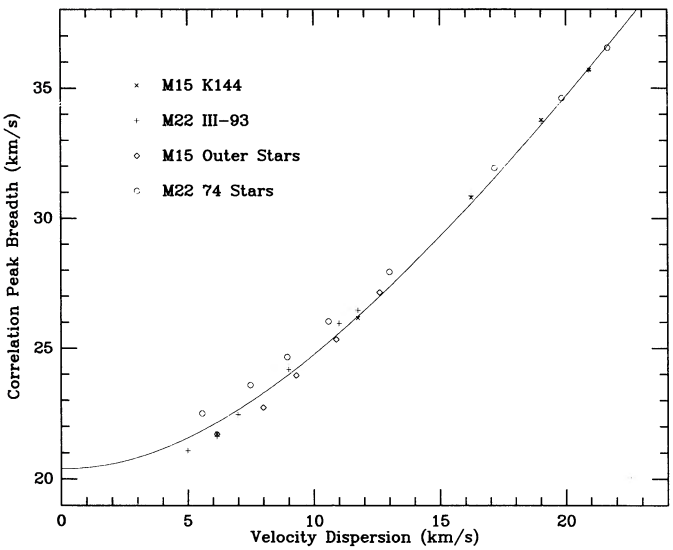

FIG. 11.—The relationship between correlation peak breadth and intrinsic velocity dispersion is presented for the MMT echelle data. Individual points mark the breadths deduced from specific spectra after broadening by dispersions of fixed amounts and incorporating in quadrature the intrinsic dispersion of the composite spectra. The small scatter of points about the mean suggests that only at the very lowest dispersions is the intrinsic stellar line strength important to the deduced velocity dispersion, at least among metal-poor giants.

Figure 4 was convolved with Gaussians corresponding to intrinsic 1 σ stellar velocity dispersions of $\sigma_i = 5$, 7, 9, and 11 km s^{-1}. The composite spectrum formed from the 59 M15 members was convolved by an additional $\sigma_i = 10$, 15, 18, and 20 km s^{-1}. The 15 km s^{-1} convolution is shown in Figure 6.

The resulting breadths are plotted against the intrinsic Gaussian dispersions in Figure 11. The final empirical relationship between peak width and velocity dispersion is the solid line drawn in Figure 11, which was used for all the MMT spectra. A separate curve for the KPNO data was determined by following the same procedure applied to KPNO spectra of K144.

Random errors in peak breadths are somewhat more difficult to judge than those of velocities. According to Tonry and Davis (1979), the uncertainty in peak breadth is the same as that in velocity, when both are expressed in pixels. However, this strictly applies only to Gaussian profiles. We have estimated the errors for these somewhat non-Gaussian profiles empirically, by determining deviations of star breadths at low R values. For stars with $R = 6$, the breadths deviate by about 20% more than the Tonry and Davis prescription would suggest. Also, the four measurements of position C, for which $R = 5$, show a scatter 15% larger. Consequently, we have determined the errors in velocity dispersion presented in Table 4 by multiplying $K/(1 + R)$ by the ratio of observed to sharp-lined peak breadth, then increasing this by 15%, then converting from breadth in pixels to dispersion in km s^{-1}.

Table 4 presents random errors of measurement only. The total uncertainty in the velocity dispersion from the central spectra is dominated in all cases by the sampling error, i.e., the small number of stars expected within a 1.″2 aperture or 1″ slit, discussed below.

c) *Line Strengths of the Central Spectrum*

Before estimating numbers of stars contributing to the central light, we first establish that the light at the center is due to essentially normal M15 giants. This inference is drawn from a comparison of the central spectrum with the one convolved from the 59 outer M15 giants. The agreement of Figures 5 and 6 leads to this conclusion, especially when the strengths of individual features are compared.

The spectral signature of cool, metal-poor giants is that lines of once-ionized species (Ti II, Fe II) and the low-excitation lines of neutral species are strong, and the Mg b lines have weak wings. In cool dwarfs of the same low metallicity, the Mg b lines have broad damping wings, and the ionized lines are extremely weak. In turnoff stars, the Cr I and Ti I lines are extremely weak.

In the central spectrum, lines of Ti II at 5188.70 Å, Ti I at 5210.39 Å, and Cr I at 5206.04 and 5208.43 Å can all be detected. Furthermore, these features plus the Mg b lines at 5167.33, 5172.70, and 5183.62 Å are the same strength in the central spectrum as in the broadened composite spectrum. This indicates that giants are the primary contributors to the integrated light.

This is consistent with the luminosity function along the giant and turnoff branches in an annulus farther from the center. Buonanno *et al.* (1983) have tabulated UBV magnitudes for all stars with $B < 18.6$ in an annulus 1.′9–5.′0 from the center of M15, deconvolving moderately blended images with Gaussians to improve the completeness of the sample at faint magnitudes. Excluding all stars away from the principal sequences, as well as all blue horizontal-branch stars (whose weak lines contribute little to the cross-correlation peak), we counted a total of 525 stars in 0.4 mag bins. A straight line fit to a plot of $d \log N$ versus V for $14 < V < 17.5$ has a slope of 0.25, i.e., a change of a factor of 10 in N over four V magnitudes. This slope is not as steep as that found for NGC 6752 by Buonanno *et al.* (1986), for which N changes by a factor of 10 over a 3 mag change in V, which supports previous suggestions that the turnoff stars are stronger contributors in clusters of higher metallicity. Here we find that roughly one-fourth of the mean V light comes from giants with $V < 13.8$, one-fourth from $13.8 < V < 14.5$, one-fourth from $14.6 < V < 15.6$, and one-fourth from $15.6 < V < 18.0$. The total additional contribution is less than 10% of that of the giant branch.

Thus the central spectrum appears to be that of a normal M15 giant branch broadened by an intrinsic velocity dispersion. There is no evidence for a hot or otherwise lineless component at the 10% level, judging from the agreement in line strengths between Figures 6 and 8.

d) *Statistical Error Due to a Small Sample*

Armed with the knowledge that the luminosity function away from the center is valid in the cusp as well, we may use it along with the apparent brightness of the cusp to estimate the error due to sampling statistics. For $V = 13$ within a 1.″2 aperture, the total number of stars binned by magnitude would average 0.2, 0.9, 1.7, and 7 for stars with $V < 13.8$, $13.8 < V < 14.5$, $14.6 < V < 15.6$, and $15.6 < V < 18.0$, respectively. Given such small numbers in the brighter bins, a statistical estimate of the sampling error is virtually meaningless, because the distribution is skewed towards a few stars whose presence or absence is crucial. Suffice it to say that one-half the samples of such a population will be dominated by one or two stars and will be roughly 50%–100% brighter than the other half.

This is consistent with the dispersion results of Table 4. Of the five positions observed in 1987 May, four have produced

velocity dispersions that are too small, i.e., lower than the disperson measured from individual stars just outside the center. We attribute this to the dominance of one or two bright stars, since the correlation results tend to favor the cold component.

The repeatability of pairs of measurements made the same night is much better than the repeatability of measurements of the same spot made on different nights. Even when great attention was paid to the precision of pointing, differences appear which are larger than expected from random errors alone. This is undoubtedly due to the effect of variations in pointing, tracking, and seeing in an extremely crowded field. Position and tracking are obviously crucial from Figures 1–3; seeing variations can affect the dispersion dramatically at a given position, since poorer seeing enhances the spillover of light from an adjacent bright star.

The long-slit data are invaluable here, since the spatial variation of the dispersion can be evaluated from simultaneous spectra. The pair of spectra at PA = 50°.1 pass through AC 216, where the dispersion is indistinguishable from that of a single star; it increases steadily to a maximum of 23 ± 3 km s^{-1} 2″ NE. In the PA = 140°.1 spectrum shown in Figure 7, broad lines are evident over a large portion of the frame. The highest cross-correlation breadths are found at pixels 77–79, just outside the central conglomeration and approximately coincident with position A in Figure 1, where the MMT dispersion also is large. Values of 21 ± 4 and 22 ± 5 km s^{-1} are deduced from the two members of this pair. Bright stars of small velocity dispersion falling at the edges of the slit could not induce a value this high, since the most broadening that an off-center position within the slit can introduce is half the spectral resolution, or ± 5 km s^{-1}.

We conclude that the low values measured for the central dispersion are those dominated by one or two stars, and that the higher values are more representative of the dispersion of the background light. Without long-slit spectra obtained in better seeing it is impossible to say exactly where the dispersion reaches a maximum, and what that value is. We take 25 km s^{-1} as a lower limit, since values this high were found both at the MMT and at KPNO each night the observations were attempted.

To compute the sampling error associated with this limit, let us conservatively take $N = 6$ stars per spectrum. The fractional sampling error in the velocity dispersion is $1/\sqrt{2N}$ or 29%. The lower limit to the intrinsic velocity dispersion then becomes 25 ± 7 km s^{-1}.

V. ASPECTS OF THE VELOCITY DISPERSION

a) Mean Values

For the cluster mean velocity, the unweighted average of the 120 cluster stars is -107.1 km s^{-1}, with a total uncertainty of ± 0.9 km s^{-1}, given an internal uncertainty of 0.8 km s^{-1} based on the scatter of the velocities about the mean, and an estimated zero-point error of 0.5 km s^{-1}. The global velocity dispersion is 9.0 ± 0.6 km s^{-1}. Webbink (1985) inferred a central velocity dispersion of 8.55 km s^{-1} if $M/L = 1.7$. Thus the global M/L of M15 is probably between 1.5 and 2.0, consistent with all other globular clusters studied to date (Peterson and Latham 1986; Pryor *et al.* 1989).

b) Rotation

Rotation has been detected in a few well-studied globular clusters at a level which may affect the dispersion in the inner regions. Invariably, it is seen in flattened clusters, and its size depends on radial distance. Meylan and Mayor (1986) find maximum $v_{\rm rot} \sin i$ values of 8 km s^{-1} in ω Centauri between 3–4 core radii r_c, and 6.5 km s^{-1} at 11–12 r_c in 47 Tucanae. The mean ellipticity is 0.121 for ω Cen and 0.099 for 47 Tuc (Geyer, Hopp, and Nelles 1983).

With poorer data for M15, Geyer *et al.* find a marginal ellipticity of 0.1 for stars 30″–61″ from the center. Possible ellipticity in the 8″ square central region is seen in Figure 2 of Newell and O'Neil (1978), but sampling statistics limit the significance of this. Moderate rotation if any is thus expected in M15.

We have looked for rotation by plotting the individual stellar velocities against position angle θ on the sky. There is no evidence for mean global rotation, as seen in Figure 12 which plots all stars regardless of radius. Given the spread in velocities, we estimate a limit for $v_{\rm rot} \sin i \lesssim 4$ km s^{-1}. A least-squares fit to a sine wave, using the nonlinear least-squares algorithm of Levenberg and Marquardt as given by Press *et al.* (1986), with measurements and sampling errors both included, gives $v_{\rm rot} \sin i \lesssim 2.5$ km s^{-1}.

Upon division into annuli, our velocities still reveal no rotation. The 57 stars interior to 1′.2, shown in Figure 13, place an upper limit of $v_{\rm rot} \sin i \lesssim 8$ km s^{-1}, because of the larger velocity dispersion of these stars. The 37 stars from 1′.2 to 2′.5 set a limit of $v_{\rm rot} \sin i \lesssim 2$ km s^{-1}, as seen in Figure 14. Least-squares fits yield 5 and 1 km s^{-1}, respectively.

In the very core, the long-slit spectra are the best guide. Figure 7 is suggestive of rotation of ≈ 10 km s^{-1} over the central 10″ region, but higher S/N spectra in excellent seeing are essential to establish this.

c) Binaries

We next rule out the possibility that the central dispersion is enhanced by the binary association of a large fraction of stars. Direct evidence for the lack of binaries is provided by our pairs of radial-velocity observations obtained nearly a year apart for most of the stars closest to the center. These are the obvious

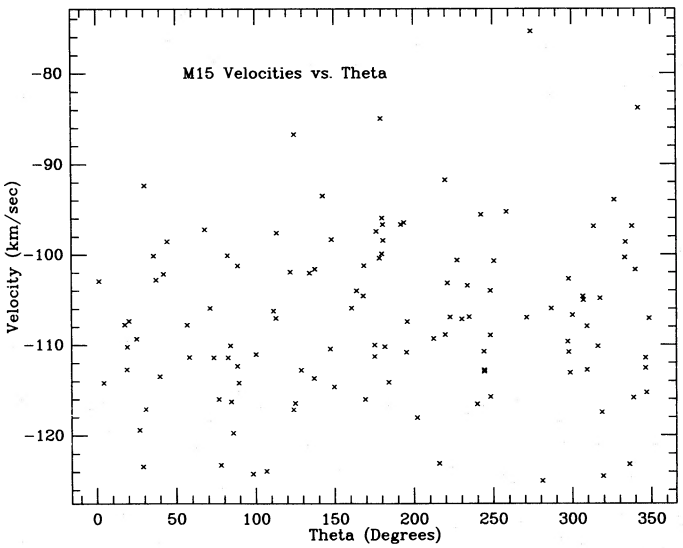

FIG. 12.—The velocities from Table 1 of 120 M15 giants are plotted against position angle to test for global rotation. None is detected at the 4 km s^{-1} level.

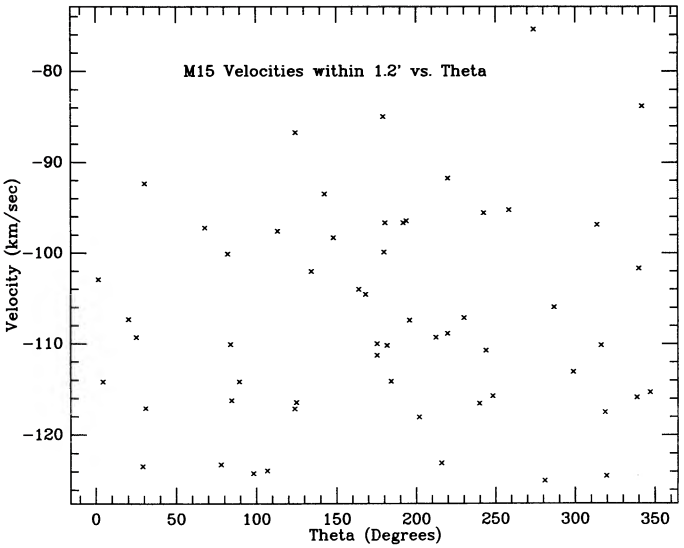

FIG. 13.—The velocities of stars interior to 1.2 are plotted against position angle. The upper limit on rotation is higher, about 8 km s^{-1}, owing to the larger velocity dispersion of the central stars.

binary candidates, since hard binaries are expected to form nearer the center. However, the 13 repeat measurements of stars within 20″ of the center all agree to a few km s^{-1}, within the expected uncertainties; the largest individual discrepancy is 3.7 km s^{-1} for AC 1. The joint deviation expected theoretically is 1.6 km s^{-1}, which is consistent with that observed, 1.8 km s^{-1}. If one were to take the difference literally, it would imply an internal variation of 0.88 km s^{-1}, consistent with the "jitter" first noted among bright giants in M3 by Gunn and Griffin (1979).

The fact that giants dominate the central spectrum argues against the presence of large numbers of short-period binaries, because their large radii would show significant rotation. At an orbital velocity of 22 km s^{-1}, for which the orbital period is <1 yr, a giant with a companion of its own mass or less would be separated from it by <1 AU, i.e., less than its own radius. Coalescence is believed to ensue, resulting in an FK Comae type of K giant. The rather rapid rotational velocity, typically 30–100 km s^{-1} (Bopp and Stencel 1981; Harris and McClure 1985), is broader than what is seen.

The central spectrum cannot be due to a single luminous FK Comae giant: to be bright enough, such a star would have a much larger radius than the typical M15 giant included in Figure 5. This would lead to stronger Ti II and Fe II lines in the central spectra, in conflict with what is observed.

d) Comparison of Velocities with a Gaussian Distribution

The largest velocity difference exhibited by a single star with respect to the mean is that of AC 224, 31.7 km s^{-1}, about twice the local dispersion or 3 times the global one. Its presence is entirely consistent with our sample size, and its velocity is still less than Webbink's central escape velocity of 41 km s^{-1}.

To examine more closely whether the central velocities are distributed consistently with a Gaussian, we have performed K-S tests on stars as a function of radius. The probability that the velocities of stars in annular groups are drawn from a Gaussian increases as radius increases, from 79% for the interior 27 stars, to 86% for the next 30, to 94% for the next 32, to 98% for the outermost 31 stars. In each case the probability is calculated using the mean and dispersion which best fits the sample under consideration. Larger samples are necessary to determine whether the innermost stars are truly deviant.

VI. THE RADIAL DEPENDENCE OF THE VELOCITY DISPERSION COMPARED TO THEORETICAL MODELS

With the above velocities and the lower limit to central dispersion, we can now examine the overall behavior of the velocity dispersion. Figure 15 plots the 120 individual stellar velocities as a function of distance from the center. By averag-

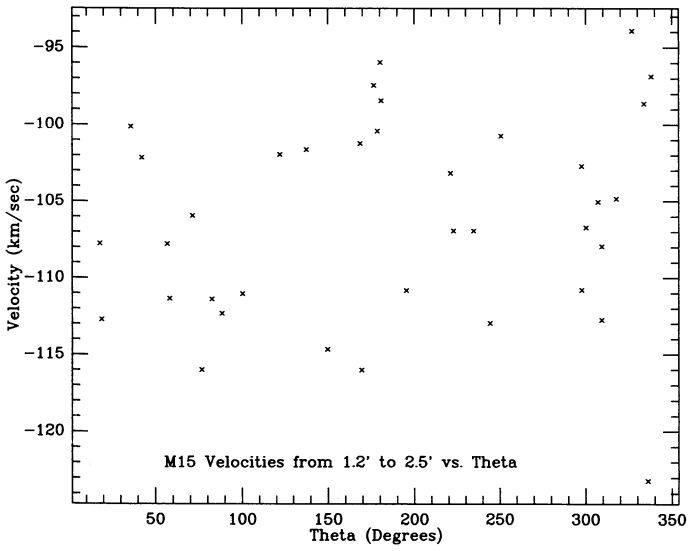

FIG. 14

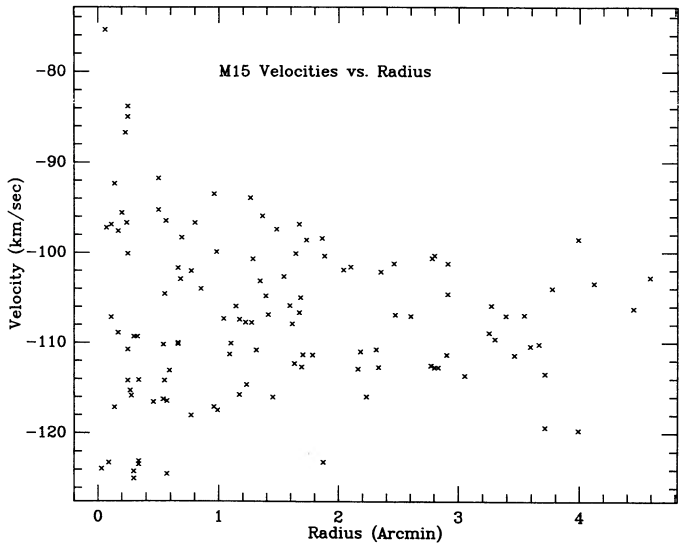

FIG. 15

FIG. 14.—The velocities of stars between 1.2 and 2.5 are plotted against position angle. Again no rotation is seen, at roughly the 2 km s^{-1} level.

FIG. 15.—The velocities from Table 1 of all 120 M15 giants are plotted against distance from the center. The spread in velocities clearly increases towards the center. The most extreme velocity difference is still less than the escape velocity from the center of the cluster.

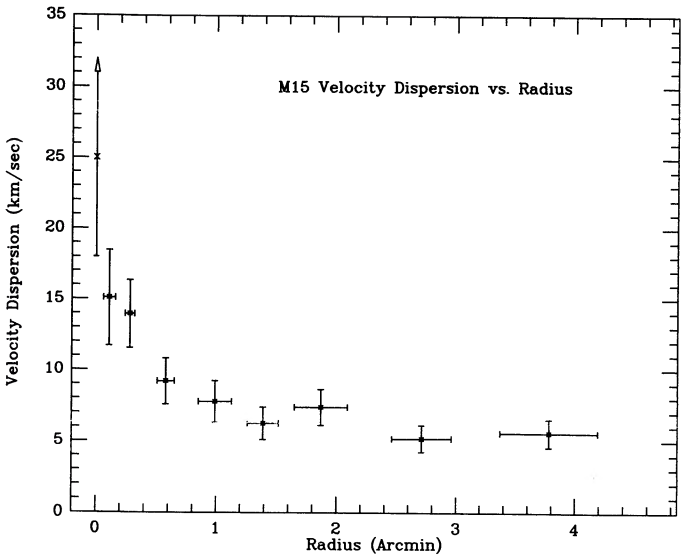

FIG. 16.—The average velocity dispersion is plotted versus radius to delineate the radial behavior of the dispersion. The X at the center marks the lower limit of 25 km s^{-1} deduced from the integrated-light spectra, and the vertical error bar indicates the sampling error assuming a total of only six stars contributes to this. The remaining points are averages of individual velocities binned by radius and are independent of one another. The horizontal error bars show the deviation in radius of the stars included in each bin, and the vertical error bars indicate the sampling error of the number of stars included. Both the integrated light dispersion and that of the individual stars near the center indicate a rise in the dispersion within 30″ of the center.

ing stars within a given annulus, the trend of the dispersion with radius can be quantified. This is represented in Figure 16. Each bin is independent of the next; the horizontal error bars indicate the 1 σ range in radius, within which $\frac{2}{3}$ of the stars fall. The vertical error bars show the statistical uncertainty due to the sample of N stars, $1/\sqrt{2N}$; proceeding from the innermost bin outward, $N = 10, 17, 16, 14, 15, 17, 15$, and 16. In each case, the dispersion computed was that with respect to the internal mean velocity of the group, rather than the velocity average of all stars.

Plotted at zero is our estimate of 25 ± 7 km s^{-1} for the lower limit to the central velocity dispersion. We believe this value is trustworthy for several reasons. A dispersion this large was detected in both KPNO long-slit CCD spectra and in MMT Reticon spectra, and is considerably higher than the instrumental resolution of 10 km s^{-1} of each system. We have presented arguments that our central value is not completely dominated by the small sample, nor is it due to stellar rotation or binaries. Since the line strengths of the central spectrum are those of normal M15 giants, the broadening is not due to a mismatch between object and template. Broad lines are unmistakably present in the background light shown in Figure 7.

The central rise is seen in the individual stellar measurements as well. The average of the first two bins differs from the average of the third and fourth bins by 2.6 times the mutual 1 σ standard deviation.

The normal procedure at this point is to compare the run of velocity dispersion versus radius with a King model whose concentration and core radius are determined from the light profile. However, the departure of the light distribution from the fit of standard King models means that the core radius r_c is not well defined; the range of values reflects various fitting compromises. Peterson and King (1975) found $r_c = 13''.8$; Hertz and Grindlay (1985) deduced 5″.5, the value adopted by Webbink (1985); and the 2.0 $M_\odot$ neutron-star model plotted in Figure 1 of Illingworth and King (1977) has $r_c = 0''.5$. At a cluster distance of 10 kpc (see, e.g., Trefzger *et al.* 1983), 5″.5 corresponds to 0.28 pc, near the lower end of the range for Galactic globulars (Webbink 1985).

No matter what r_c is chosen, the relaxation time near the cluster center is very short. Taking the central surface density calculated by Webbink (1985), the central relaxation time scale as defined by Peterson and King (1975) is only 14×10^6 yr. Given such a short relaxation time, the assumption of thermal equilibrium should hold whether or not mass segregation is included in isothermal models, since it demands energy equipartition not only between stars of different masses but also between stars of the same mass at adjacent radii. The several M15 King models, including those with mass segregation such as the neutron-star model of Illingworth and King (1977), and the recently refined M15 model of King (1989) do predict somewhat different dependences of velocity dispersion on radius. However, they all share a dispersion which is flat out to 30″ or more, and then falls progressively more steeply toward larger radii.

Our results are not consistent with this. Instead, the one-dimensional velocity dispersion is seen to rise gradually at large radial distances and precipitously near the center. The dispersion changes by a factor <2 over a factor of 8 in radius, then is twice as large right at the center. We conclude that the velocity distribution at the very center must be nonisothermal.

The mass-to-light ratio near the center is extremely model-dependent. The global value of $M/L_V \sim 2$ holds in the outer regions.

Could the central velocities be predominantly radial? We think not, for even in a nonisothermal model, the short relaxation time argues against preferentially radial orbits. One might postulate that a slingshot mechanism such as scattering off a hard binary regenerates radial orbits on an equally short time scale. However, it is difficult to see how a significant number of objects would acquire a moderately high velocity but none a very high one, and how such a population is sustained against its own collapse.

Laying aside stability considerations for the moment, it is worthwhile to ask whether a single central potential can consistently produce both the surface density cusp in the light profile and the central rise in velocity dispersion. Larson (1984) has postulated a singular central density distribution in an otherwise normal cluster model, constructing models with two mass classes dominated at the center by heavy remnants. One of his models, with the heavy stellar mass twice the lighter and $r_c = 2''.6$, provides an adequate fit to the light profile of M15. Larson assumed for both mass classes a space density $\rho \sim r^{-2.5}$, so that $\sigma^2 \sim r^{-0.5}$ in his model. The central rise he predicts is therefore somewhat smaller than what we observe as a lower limit; for reasons discussed above with respect to King models, there may also be some difficulty with the relative constancy of the observed dispersion between 15 and 90 r_c. Moreover, dynamical calculations presented by Cohn (1985) suggest that Larson's assumed density dependence may be optimistic. Cohn's Figure 4, which presents the evolution of his own two-mass model with the same mass ratio, shows that the two components exhibit a different radial dependence due to mass segregation. For the steeper dependence (that of the heavy component) $\rho \sim r^{-2.2}$, and so $\sigma^2 \sim r^{-0.2}$. The observed cusp in surface brightness is suppressed further by the weaker

radial dependence of the density of the less massive component.

The approach to core collapse and its dynamical consequences, along with other aspects of the internal dynamics of globular clusters, are well surveyed by Elson, Hut, and Inagaki (1987). It is now widely held that the stability of clusters against collapse is strongly influenced by binaries. As reviewed by Spitzer (1985) and Heggie (1985), or summarized for example by McMillan (1986), core collapse is halted by the emission of energy as a hard binary becomes harder in collisions with single stars or a less hard binary, for such a collision generally imparts kinetic energy to the unbound or weakly-bound system. At late stages the number of stars remaining in the core is small, <100, and is dominated by from zero to a few binaries. Substantial theoretical effort is currently devoted to their effect on the energy flux from the hotter core.

Unfortunately few explicit results are available for the central velocity distribution of post–core-collapse models. Those that exist do not currently offer much hope of explaining our M15 results. For example, Figure 16 of Statler, Ostriker, and Cohn (1987), which includes the influence of tidal-capture binaries, suggests an increase of less than a factor of 2 in the central velocity dispersion, and this only during the extremely brief epoch of core collapse. The work of Goodman (1987) on gravothermal oscillations also indicates that increases in the central velocity dispersion are of short duration. Brief velocity enhancements of small amplitude appear to be typical of post–core-collapse models with binaries as a central heat source. Evidently what is needed is a mechanism which greatly increases the rate of local heat input over longer times.

An alternative scenario is that the presence of a black hole that has grown from a small "seed" may reverse core collapse, through consumption or ejection of stars in the cusp. According to Marchant and Shapiro (1980) and Duncan and Shapiro (1982), such a black hole in a globular cluster grows to about 1000 $M_\odot$; a stable situation ensues in which the velocity dispersion rises abruptly very near the radius where the light cusp also begins, and reaches very large values right at the center. These results, based on Monte Carlo simulations, have also been produced in Fokker-Planck computations. Cohn (1985, pp. 171–172) reports that he has incorporated a seed black hole of 50 $M_\odot$ into a cluster of 3×10^5 $M_\odot$ and applied his one-dimensional orbit-averaged Fokker-Planck code to the subsequent evolution. After 21×10^{10} yr, core collapse plus accretion led to a cusp of 0.1 r_c extent. Late post–core-collapse evolution led to a mass of 3×10^3 $M_\odot$ for the black hole. He noted that the predominant signature of the presence of a single massive black hole is that the velocity dispersion depends very steeply on radius: $\sigma^2 \sim r^{-1}$.

These calculations would appear to be in generally excellent agreement with our observations. The three innermost velocity dispersion points based on individual stars follow Cohn's predicted dependence extremely well; the central rise inferred from integrated light is also consistent. The mass implied for a central black hole is about 1000 $M_\odot$. Also, the overall behavior of the central region of M15, namely an abrupt increase in the light profile and the velocity dispersion, is strikingly similar to what is seen very near the centers of the nearby galaxies Andromeda (M31) and its compact elliptical companion M32, for which massive black holes are frequently invoked (e.g. Tonry 1984; Dressler 1984; Kormendy 1986).

Before carrying this further, however, it is critical to establish over what range and how rapidly the velocity dispersion increases near the center, and to clearly determine to what extent rotation may be present in the vicinity. This will entail measurements of the velocity and velocity dispersion at several positions near the center under conditions of excellent seeing. An independent investigation of the behavior of the velocity dispersion near the center of other cusp clusters would also be worthwhile, to determine whether a high central velocity dispersion is a common phenomenon in such cases.

We are especially pleased to thank Ivan King for his long-standing interest in this work and for many informative discussions concerning it. We are also grateful to Lee Hartmann for obtaining data at our request; to Bob McClure for providing the CFHT CCD frame of the M15 central region in advance of publication; and to the CfA TAC for repeated allocations of MMT time. The difficulty of working in crowded fields was alleviated by the skill of telescope operators Carol Heller, John McAfee, and Janet Robinson at the MMT and George Will at KPNO; and by the precision of the pointing of the MMT, for which we are indebted to the MMT staff. We thank Frank Sharp and Kirk Gilmore for the effective implementation of the remote-observing microwave link, and Gilmore and Bill Wyatt for help in the conversion of IRAF FITS-format spectra to Mount Hopkins correlation format. R. C. P. was supported by NSF grant AST 85-21487 during the initial stages of this work. The research of K. M. C. on this project was also partially supported by NSF.

REFERENCES

Arp, H. C. 1955, *A.J.*, **60**, 317.
Aurière, M., and Cordoni, J.-P. 1981, *Astr. Ap. Suppl.*, **46**, 347 (AC).
Aurière, M., Le Fèvre, O., and Terzan, A. 1984, *Astr. Ap.*, **138**, 415.
Bopp, B. W., and Stencel, R. E. 1981, *Ap. J.*, **249**, 662.
Brown, A. 1951, *Ap. J.*, **113**, 344.
Buonanno, R., Buscema, G., Corsi, C. E., Iannicola, G., and Fusi Pecci, F. 1983, *Astr. Ap. Suppl.*, **51**, 83.
Buonanno, R., Caloi, V., Castellani, V., Corsi, C., Fusi Pecci, F., and Gratton, R. 1986, *Astr. Ap. Suppl.*, **66**, 79.
Buonanno, R., Corsi, C. E., and Fusi Pecci, F. 1985, *Astr. Ap.*, **145**, 97.
Cohn, H. 1985, in *IAU Symposium 113, Dynamics of Star Clusters*, ed. J. Goodman and P. Hut (Dordrecht: Reidel), p. 161.
Cudworth, K. M. 1976, *A.J.*, **81**, 519.
Djorgovski, S., and King, I. R. 1984, *Ap. J. (Letters)*, **277**, L49.
Dressler, A. 1984, *Ap. J.*, **286**, 97.
Duncan, M. J., and Shapiro, S. L. 1982, *Ap. J.*, **253**, 921.
Elson, R., Hut, P., and Inagaki, S. 1987, *Ann. Rev. Astr. Ap.*, **25**, 565.
Federici, L., Fusi Pecci, F., Zavaroni, C., Buonanno, R., Corsi, C. E., Quintiliani, A., and Epps Bingham, E. A. 1983, *Ap. Space Sci.*, **90**, 405.
Geyer, E. H., Hopp, U., and Nelles, B. 1983, *Astr. Ap.*, **125**, 359.
Goodman, J. 1987, *Ap. J.*, **313**, 576.
Gunn, J. E., and Griffin, R. F. 1979, *A.J.*, **84**, 752.
Harris, H. C., and McClure, R. D. 1985, *Pub. A.S.P.*, **97**, 261.
Heggie, D. C. 1985, in *IAU Symposium 113, Dynamics of Star Clusters*, ed. J. Goodman and P. Hut (Dordrecht: Reidel), p. 139.
Hertz, P., and Grindlay, J. E. 1983, *Ap. J.*, **275**, 105.
———. 1985, *Ap. J.*, **298**, 95.
Illingworth, G. 1976, *Ap. J.*, **204**, 73.
Illingworth, G., and King, I. R. 1977, *Ap. J. (Letters)*, **218**, L109.
King, I. R. 1966, *A.J.*, **71**, 64.
———. 1985, in *IAU Symposium 113, Dynamics of Star Clusters*, ed. J. Goodman and P. Hut (Dordrecht: Reidel), p. 1.
———. 1989, in *Dynamics of Dense Stellar Systems*, ed. D. Merritt (Cambridge: Cambridge University Press), p. 157.
Kormendy, J. 1986, in *Supermassive Black Holes*, ed. M. Kafatos (Cambridge: Cambridge University Press), p. 98.
Küstner, F. 1921, *Veröff. Sternw. Bonn.*, No. 15.
Larson, R. B. 1984, *M.N.R.A.S.*, **210**, 763.
Latham, D. W. 1985, in *IAU Colloquium 88, Stellar Radial Velocities*, ed. A. G. D. Philip and D. W. Latham (Schenectady: L. Davis), p. 21.
Marchant, A. B., and Shapiro, S. L. 1980, *Ap. J.*, **239**, 685.
McClure, R., Racine, R., and Christian, C. 1989, *CFH Bulletin*, No. 20, p. 5.

McMillan, S. L. W. 1986, *Ap. J.*, **307**, 126.
Meylan, G., and Mayor, M. 1986, *Astr. Ap.*, **166**, 122.
Newell, B., Da Costa, G. S., and Norris, J. 1976, *Ap. J. (Letters)*, **208**, L55.
Newell, B., and O'Neil, E. J., Jr. 1978, *Ap. J. Suppl.*, **37**, 27.
Peterson, C. J., and King, I. R. 1975, *A.J.*, **80**, 427.
Peterson, R. C. 1983, *Ap. J.*, **275**, 737.
Peterson, R. C., and Cudworth, K. M. 1989, in preparation.
Peterson, R. C., and Latham, D. W. 1986, *Ap. J.*, **305**, 645.
Peterson, R. C., Olszewski, E. W., and Aaronson, M. 1986, *Ap. J.*, **307**, 139.
Press, W. H., Flannery, P. F., Teukolsky, S. A., and Vetterling, W. T. 1986, *Numerical Recipes* (Cambridge: Cambridge University Press), pp. 532–537.
Pryor, C. P., Latham, D. W., and Hazen, M. L. 1988, *A.J.*, **96**, 123.
Pryor, C. P., McClure, R., Fletcher, J. M., and Hesser, J. E. 1989, in preparation.
Sandage, A. 1970, *Ap. J.*, **162**, 841.
Spitzer, L., Jr. 1985, in *IAU Symposium 113, Dynamics of Star Clusters*, ed. J. Goodman and P. Hut (Dordrecht: Reidel), p. 109.
Statler, T. S., Ostriker, J. P., and Cohn, H. N. 1987, *Ap. J.*, **316**, 626.
Tonry, J. L. 1984, *Ap. J. (Letters)*, **283**, L27.
Tonry, J., and Davis, M. 1979, *A.J.*, **84**, 1511.
Trefzger, C. F., Carbon, D. F., Langer, G. E., Suntzeff, N. B., and Kraft, R. P. 1983, *Ap. J.*, **266**, 144.
Webbink, R. F. 1985, in *IAU Symposium 113, Dynamics of Star Clusters*, ed. J. Goodman and P. Hut (Dordrecht: Reidel), p. 541.
Wolszczan, A., Kulkarni, S. R., Middleditch, J., Backer, D. C., Fruchter, A. S., and Dewey, R. J. 1989, *Nature*, **337**, 531.
Wyatt, W. F. 1985, in *IAU Colloquium 88, Stellar Radial Velocities*, ed. A. G. D. Philip and D. W. Latham (Schenectady: L. Davis), p. 123.

KYLE M. CUDWORTH: Yerkes Observatory, University of Chicago, P.O. Box 258, Williams Bay, WI 53191

RUTH C. PETERSON: Smithsonian Observatory, Steward Observatory, University of Arizona, Tucson, AZ 85721

PATRICK SEITZER: Space Telescope Science Institute, 3700 San Martin Drive, Baltimore, MD 21218